Clinical Kidney Journal, 2024, vol. 17, no. 1, 1–14

https://doi.org/10.1093/ckj/sfad277
Advance Access Publication Date: 8 November 2023
Original Article

ORIGINAL ARTICLE

Single-cell transcriptomes of kidneys in a 6-month-old boy with Denys-Drash syndrome reveal stromal cell heterogeneity in the tumor microenvironment

Tao Li[1,*], Jiangfeng Zhou[1,*], Haiyan Wu[2], Xiucheng Gao[3], Qiyang Shen[4], Rui Cheng[5] and Mingshun Zhang[6]

[1]Department of Oncology Surgery, Children's Hospital of Nanjing Medical University, Nanjing, China, [2]Department of Pathology, Children's Hospital of Nanjing Medical University, Nanjing, China, [3]Department of Radiology, Children's Hospital of Nanjing Medical University, Nanjing, China, [4]Department of Pediatric Surgery, Children's Hospital of Nanjing Medical University, Nanjing, China, [5]Department of Neonatal Medical Center, Children's Hospital of Nanjing Medical University, Nanjing, China and [6]NHC Key Laboratory of antibody technique, Department of Immunology, Nanjing Medical University, Nanjing, China

*Tao Li and Jiangfeng Zhou contributed equally to this work.
Correspondence to: Rui Cheng and Mingshun Zhang; E-mails: chengrui350@163.com and mingshunzhang@njmu.edu.cn

ABSTRACT

Background. Denys-Drash syndrome (DDS) is a rare disease characterized with pseudohermaphroditism, nephroblastoma (also known as Wilms tumor), and diffuse mesangial sclerosis. The therapy for DDS is largely supportive, i.e. surgery and chemotherapy for Wilms tumor and renal replacement therapy. Due to the limited understanding of the pathogenesis, precision therapy for DDS is yet to be explored. We sought to explore the cellular components and interactions in kidney tissues from an infant with DDS.

Methods. Whole-exome sequencing was performed to examine the mutations associated with DDS. Single-cell RNA sequencing (scRNA-seq) was performed to explore the heterogenicity of kidney tissue samples.

Results. A 6-month-old infant with bilateral Wilms tumors and genital ambiguity was diagnosed as having DDS. Whole exome sequencing revealed a novel *de novo* mutation (p.F185fs*118) in exon 1 of *WT1*. scRNA-seq was performed in tissue samples from bilateral Wilms tumors and the normal kidney from this infant. Fibroblasts, myocytes, epithelial cells, endothelial cells, and mononuclear phagocytes (MPs) ranked at the top of the 31 135 total cells. Fibroblasts and myocytes were dominant in the Wilms tumor samples. In contrast, most epithelial cells and endothelial cells were found in normal kidney tissues. *CD44* and *TUBA1A* were significantly changed in myocyte subclusters, which may contribute to chemotherapy drug resistance. Macrophages intensively interacted with cancerous cells, including fibroblasts, epithelial cells, and myocytes.

Conclusions. A novel mutation (p.F185fs*118) in exon 1 of *WT1* was identified in an infant with DDS. scRNA-Seq revealed the heterogenicity of cellular components in Wilms tumors and kidney tissues, shedding light on the pathogenesis of DDS.

Received: 19.3.2023; Editorial decision: 24.10.2023

GRAPHICAL ABSTRACT

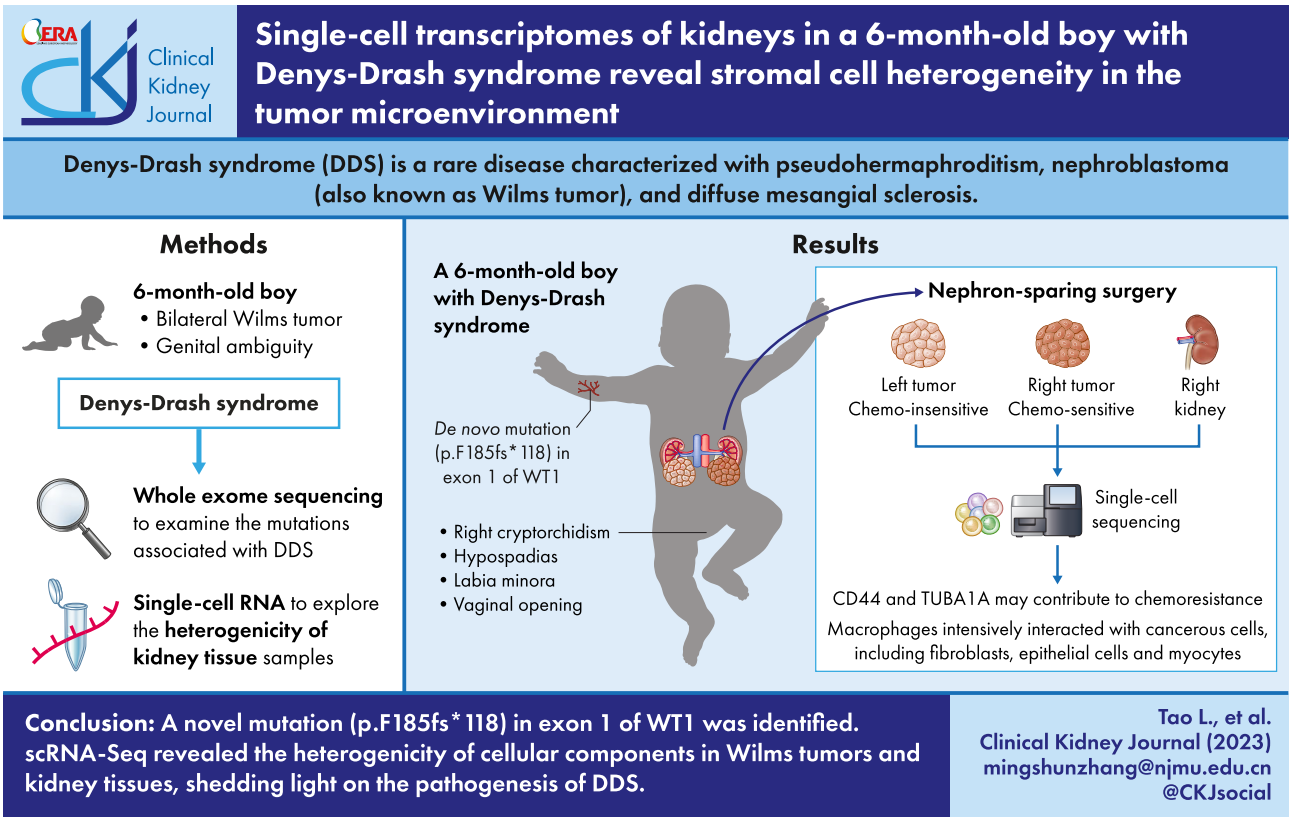

Keywords: Denys-Drash syndrome, single-cell RNA-Seq, tumor microenvironment, whole exome sequencing, Wilms tumor

KEY LEARNING POINTS

What was known:

- Denys-Drash syndrome (DDS) is a rare disease in infants characterized with pseudohermaphroditism, nephroblastoma (also known as Wilms tumor), and diffuse mesangial sclerosis.
- The therapy for DDS is largely supportive, i.e. surgery and chemotherapy for Wilms tumor and renal replacement therapy.
- The cellular heterogeneity in kidney and Wilms tumor tissues from DDS remain elusive.

This study adds:

- A novel *de novo* mutation (p.F185fs*118) in exon 1 of WT1 was identified in a DDS infant.
- Single-cell RNA sequencing (scRNA-seq) was performed to explore the heterogenicity of kidney tissue samples.
- CD44 and TUBA1A were significantly changed in myocyte subclusters, which may contribute to chemotherapy drug resistance.

Potential impact:

- scRNA-seq is a valuable tool to explore the pathogenesis of rare diseases and the precision oncology.
- Application of multi-omics may provide clues to potential gene therapy for DDS and other rare diseases.

INTRODUCTION

Denys-Drash syndrome (DDS) is a rare disease that begins within the first few months of life [1]. The common clinical features for complete DDS include pseudohermaphroditism, nephroblastoma (also known as Wilms tumor), and diffuse mesangial sclerosis. The boy with DDS is normal in sex chromosomes (XY), but the external genitals are ambiguous. Wilms tumor is the most frequent kidney cancer in children [2]. Most Wilms tumors are isolated, and approximately 5% of Wilms tumors may occur accompanied by other syndromes, i.e. DDS. Although rare, DDS may vary in clinical characteristics. Incomplete DDS, defined as nephropathy with genital anomalies or Wilms tumor, has also

been reported [3]. In addition, an infant who presented with bilateral Wilms tumor and genital ambiguity without nephropathy was diagnosed with DDS [4]. However, Wilms tumor alone without mesangial sclerosis and genital anomalies excluded DDS [5]. The therapy for DDS is supportive, i.e. surgery and chemotherapy for Wilms tumor and renal replacement therapy. The prognosis for children with Wilms tumor is good [6]. Due to the limited data available, the long-term outcomes for infants with DDS are not yet clear [7].

As a genetic disorder, the well-known culprits of DDS are mutations in the Wilms tumor suppressor gene, *WT1*; over 90% of DDS is linked with constitutional intragenic *WT1* mutations [3]. WT1 is required for the early development of kidneys and gonads before birth [8]. Podocyte maturation is delayed in DDS, in which podocytes express the proangiogenic isoform VEGF165 but lose the inhibitory isoform VEGF165b [9]. WT1 regulates the VEGF isoforms; WT1 knockout promotes the antiangiogenic VEGF120 isoform [10]. Isolated Wilms tumors and Wilms tumors in DDS may share the same WT1 mutation, i.e. R362X [5], indicating that WT1 mutations alone may not be sufficient to cause DDS. The mechanisms by which WT1 mutants regulate the pathogenesis of DDS are still largely elusive.

Regarding Wilms tumor alone, single-cell transcriptomes have been reported in few papers [11, 12]. To bridge the knowledge gap in the pathogenesis of Wilms tumor in DDS, in the present study, we provided the first single-cell study in kidney tissues from a 6-month-old DDS infant. The peripheral blood was analysed for whole exome sequencing to identify gene mutations associated with Wilms tumor and DDS. Bilateral Wilms tumor tissue samples and normal kidney tissue samples were processed for single-cell RNA sequencing. We constructed a single-cell atlas for DDS and characterized the molecular signatures of diverse cells for this rare disease.

MATERIALS AND METHODS

Clinical examinations and treatments

Abdominal swelling and vomiting caused by Wilms tumors are sometimes the first clinical signs of DDS. In the present study, a 6-month-old boy presented to the emergency department with a history of recurrent vomiting. Computed tomography (CT) scanning was performed to validate the abdominal mass and chest metastasis. Cardiac ultrasonography was used to observe the patent foramen ovale. Syphilis-specific IgG antibody in the sera was tested using the Elecsys syphilis assay (Roche Diagnostics, Indianapolis, IN, USA). Peripheral blood samples were collected for renal function tests; specifically, blood urea nitrogen and creatinine were measured.

The patient was treated with a vincristine, actinomycin D and dexamethasone (VAD) regimen. Subsequently, the patient received nephron-sparing surgery, first for the Wilms tumor in the right kidney and then for the Wilms tumor in the left kidney. After the operation, the patient was treated with a VAD regimen and local radiotherapy in bilateral renal areas.

Whole exome sequencing

Genomic DNA was extracted from EDTA-treated peripheral blood using a Genomic DNA kit (DP329-TA, TIANGE, China). Exosomes were enriched using xGen exosome research panel v2.0 (IDT, Iowa, USA). High-throughput sequencing for exosomes was performed by an MGI NBSEQ-T7 sequencer. After quality control, the paired-end reads were performed using Burrows–Wheeler Aligner (BWA) to the Ensemble GRCh37/hg19 reference genome. SNPs and indels were screened, and high-quality and reliable variants were obtained. Minor allele frequencies (MAFs) were annotated using databases including 1000 genomes, dbSNP, ESP, ExAC, and genomAD. The OMIM, HGMD, and ClinVar databases were used for pathogenicity annotations. Functional changes in variants were predicted using the MaxEntScan, dbscSNV, SpliceAI, and GATAG software packages. Moreover, CANOE, CNVnator, DeviCNV, and ExosomeDepth were used to detect CNVs.

Single-cell RNA sequencing

In the first nephron-sparing surgery, Wilms tumor in the right kidney and normal kidney tissue samples were collected during surgery. Meanwhile, samples from Wilms tumor in the left kidney were punctured. The sample processing and single-cell RNA sequencing of human kidney samples have been extensively described [13]. Briefly, single cells from each tissue sample were acquired by a GEXSCOPE™ Tissue Dissociation kit (Singleron Biotechnologies, Nanjing, China). A microfluidic chip was loaded with the single-cell suspension. Guided by the manufacturer's instructions (Singleron GEXSCOPE Single Cell RNAseq Library Kit, Singleron Biotechnologies), single-cell RNA-seq libraries were prepared. Sequencing was performed on an Illumina HiSeq X10 instrument with 150-bp paired-end reads.

Single-cell bioinformation analysis

Raw reads were processed to generate mRNA profiles using an internal celescope1.3.0 pipeline. Briefly, after filtering read one without poly T tails, the cell barcode and UMI were extracted. Adapters and poly A tails were trimmed (fastp V1) before aligning read two to hg19/GRCh37with ensemble version 92 gene annotation (fastp v2.5.3a and featureCounts v1.6.2) [14]. Reads with the same cell barcode, UMI and gene were grouped together to calculate the number of UMIs per gene per cell. The UMI count tables of each cellular barcode were used for further analysis. Cell type identification and clustering analysis were performed using Seurat (v4.0.4) and clustermole (v1.1.0) [15]. The cluster assignment to cell types is decided by markers, which are listed in the Figs S1–S7 (see online supplementary material). Rigorous quality control was performed, and cells with >2500 or <200 gene features and >20% mitochondrial genes were removed. Standard Seurat workflow analysis was performed. Different samples were integrated with the IntegrateData function [16]. The parameter resolution was set to 0.15 for the FindClusters function to identify clusters. Differentially expressed genes (DEGs) between different clusters were identified with the function FindMarkers, and gene set enrichment analysis (GSEA) was performed to identify enriched pathways [17].

RESULTS

Clinical and molecular characteristics of the infant with DDS

In the physical examination, the infant was found to have an abdominal mass, right cryptorchidism, hypospadias, labia minora and vaginal opening. On the CT scan, bilateral renal masses (90 × 75 × 71 mm on the left and 89 × 83 × 81 mm on the right) were observed (Fig. 1A). Chromosome analysis revealed a

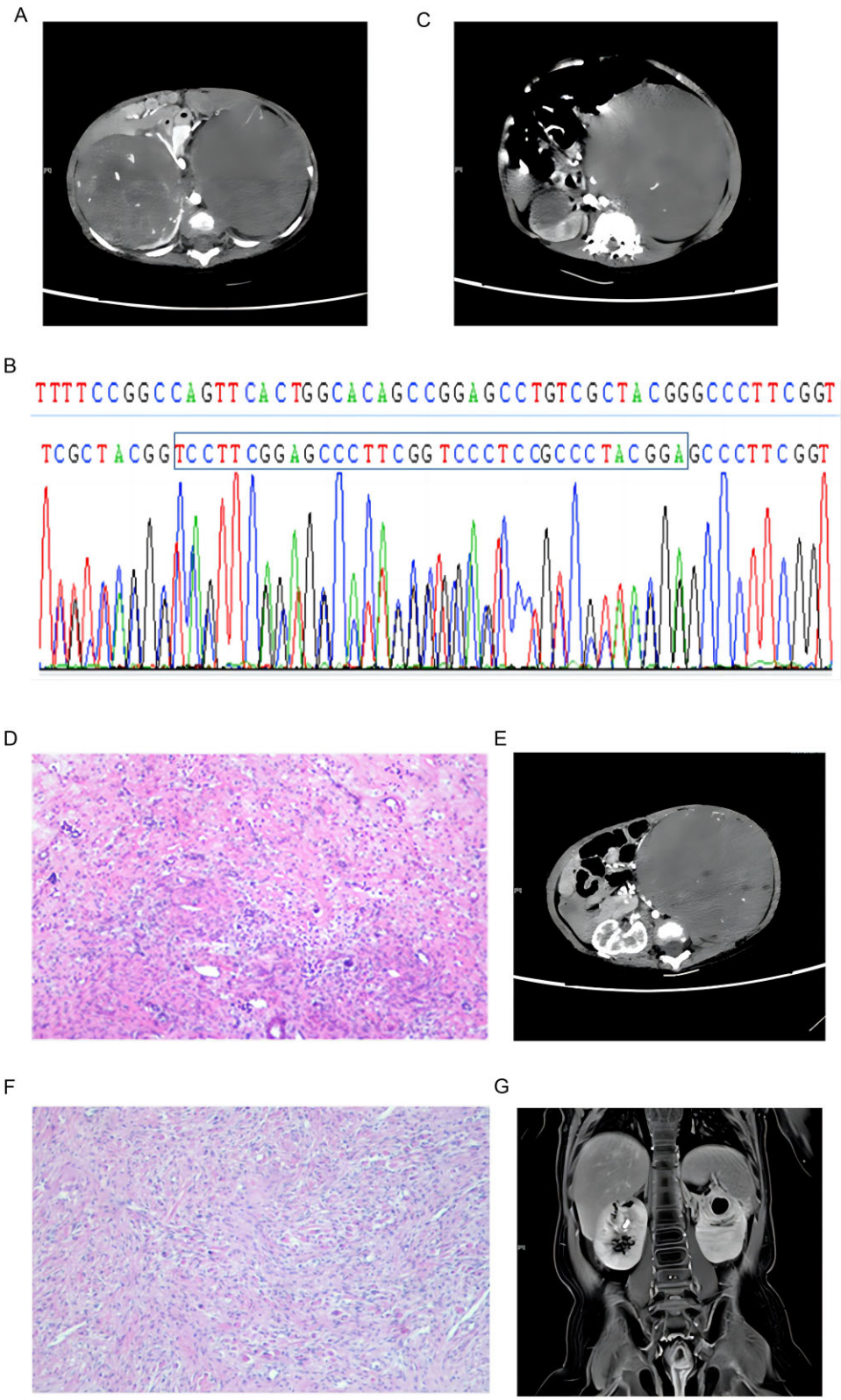

Figure 1: Clinical characteristics of the infant with DDS. **A**. Contrast-enhanced CT image in the arterial phase at the initial visit; **B**. Sanger sequencing for the insertion mutation in WT1, with an insertion mutation: c.548- 549 ins TCCTTCGGAGCCCTTCGGTCCCTCCGCTACGGA. **C**. Contrast-enhanced CT image in the arterial phase after 6 weeks of preoperative chemotherapy. **D**. Postoperative pathology of the right tumor: nephroblastoma (mainly mesenchymal type), with a large amount of proliferative fibrous tissue in the tumor and chronic inflammatory cell infiltration in the stroma. **E**. Contrast-enhanced CT image in the arterial phase before the second surgery. **F**. Postoperative pathology of the left tumor: nephroblastoma (mainly mesenchymal type), with a large amount of fusiformis mesenchymal components in the tumor and some differentiation into striated muscle. **G**. Contrast-enhanced MRI coronal images after treatment ends.

46, XY karyotype. His mother had congenital renal ectopia, and his father denied a history of severe diseases. The patient was immediately admitted to the pediatric oncology ward. Further examinations were performed during hospitalization. In the chest scan, there were no obvious metastatic lesions. On cardiac ultrasonography, a patent foramen ovale was found. In the cardiac function test, the infant seemed normal. Considering that his mother was positive for the syphilis-specific antibody IgG during pregnancy, we performed a hematologic examination and found that the syphilis antibody IgG in the infant sera was positive. In the renal function test, his urea nitrogen level was 2.4 μmol/L within the reference range (1.8∼6.5 μmol/L), and his creatinine level was 21 μmol/L, which was higher than the normal limits (8.4∼13.25 mmol).

Renal masses in the infants are often associated with Wilms tumor. To explore whether the infant had putative *WT1* mutations, we performed whole-exome sequencing (WGS) in the infant and his parents. His parents were without *WT1* mutations. In the infant, however, WGS detected a *de novo* insertion in the exon 1 of *WT1*: c.548_ 549insTCCTTCGGAGCCCTTCGGTCCCTCCGCCCTACGGA, which caused p. F185fs*118 (p. Phe185fsTer118) (Fig. 1B). The *de novo* insertion mutation caused the termination after 118 amino acids starting from Phe185, resulting in a predicted truncated protein with impaired function. According to ACMG guidelines, this novel mutation was considered pathogenic for Wilms tumor. Therefore, this 6-month-old boy with hermaphroditism and Wilms tumor was diagnosed with DDS.

The patient first received the VAD regimen for 2 courses in six weeks. According to the SIOP program, the drug dose of all children whose weight was less than 12 kg was reduced to 67%. Follow-up CT showed that the right kidney tumor size was obviously reduced to 43 × 42 × 36 mm, and the left kidney tumor was larger to 109 × 107 × 98 mm (Fig. 1C). In the renal function test, his urea nitrogen level was 2.2 μmol/L, and his creatinine level was 18 μmol/L. Following multidisciplinary discussions, we decided to perform right kidney nephron-sparing surgery and left tumor biopsy for the patient. Postoperative pathology showed that the right tumor was nephroblastoma (mainly mesenchymal type) with postchemotherapy changes (Fig. 1D). There was no obvious metastasis in the bilateral perihilar lymph nodes. During the operation, the left nephroblastoma biopsy tissue was also taken for PDTX drug screening. We re-examined renal function after the operation. Blood urea nitrogen was increased to 5.1 μmol/L, and creatinine was up to 30 μmol/L.

We continued the VAD regimen 3 weeks after the operation. Then, a CT scan showed that the left kidney tumor size increased to 109 × 107 × 98 mm (Fig. 1E). Moreover, renal function began to worsen after the operation: urea nitrogen was 1.9 μmol/L, and creatinine was 20 μmol/L. In addition, the patient began to have hypertension. Although spironolactone and captopril were administered to control blood pressure, the patient still experienced tachycardia and moderate hypertension. To prevent abdominal compartment syndrome (ACS) associated with giant nephroblastoma, we decided to perform left kidney nephron-sparing surgery. The postoperative pathology indicated that the left renal tumor was consistent with the transformation from nephroblastoma (mainly mesenchymal) to striated muscle, and no significant metastasis was found in the left hilum lymph node (Fig. 1F). Postoperative urea nitrogen was 2.6 μmol/L, and creatinine was 18 μmol/L. The blood pressure gradually returned to normal after the operation. We still used the VAD regimen in three courses for 9 weeks to treat the infant. At the end of treatment, MRI showed that the upper pole structure of both kidneys was not clear, and no obvious abnormal mass was found (Fig. 1G). In the renal function tests, urea nitrogen was 1.9 μmol/L, and creatinine was 20 μmol/L. At present, the boy has been followed up closely.

Detailed single-cell atlas in kidney and Wilms tumor tissues

To establish the cellular microenvironments of the DDS infant, we performed scRNA-seq for three kidney samples from the patient, including bilateral Wilms tumors and normal kidney tissues on the right side (Fig. 2A). After quality control and data preprocessing, 31 135 cells were retained for downstream analysis. Unbiased clustering revealed 12 cellular populations, i.e. epithelial cells, myocytes, mesangial cells, podocytes, endothelial cells (ECs), mural cells, fibroblasts, T cells, mononuclear phagocytes (MPs), plasmacytoid dendritic cells (pDCs), erythrocytes, and proliferating cells (Fig. 2B). The cell numbers in each sample and the canonical markers for each major cluster are listed in Table S1 and Fig. S1 (see online supplementary material). The distribution of these clusters was quite different in right tumor, left tumor, and normal kidney tissue samples. Fibroblasts and myocytes dominated in the Wilms tumors. In contrast, epithelial cells and endothelial cells populated the normal kidney samples (Fig. 2C). The Wilms tumors on each side also varied in cellular components. Following dimension reduction and Leiden clustering, fibroblasts in right and left Wilms tumors were visualized in different subclusters by uniform manifold approximation (UMAP). Meanwhile, myocytes were recorded only in the left Wilms tumor tissue samples (Fig. 2D). The complicated cellular components in the bilateral Wilms tumors suggested heterogenicity in cancer microenvironments. To elucidate the origin of cancer cells, we calculated the copy number variation (CNV) score in the major cell clusters (Fig. 2E–F). The CNV score in the MPs was lowest. In comparison, fibroblasts and myocytes in Wilms tumors hosted higher CNV scores, implying that these cells may be tumor cells. Most epithelial cells were from normal kidney tissues. The CNV score in the epithelial cells, however, was higher than that in MPs. We could not preclude the possibility that these epithelial cells may be cancerous. Collectively, we established a single-cell atlas with multiple cell clusters in Wilms tumors and kidney tissues for DDS.

Wilms tumor and kidney fibroblasts subcluster into distinct cell populations

Fibroblasts were the most prominent cancer cells in the bilateral Wilms tumor tissue samples (Fig. 2D; Table S1, see online supplementary material). To uncover the potential roles of fibroblasts in Wilms tumor, we subcluster 12 838 fibroblasts into five distinct populations (Fig. 3A). Subcluster 1 fibroblasts (marked by *CFD*, *SPRX*, *DPT*, etc.), subcluster 4 fibroblasts (marked by *SLPI*, *CLU*, *NDNF*, etc.) and subcluster 5 fibroblasts (marked by *C7*, *HHIP*, *ATF3*, etc.) prevailed in the right Wilms tumor sample. In contrast, subcluster 2 fibroblasts (marked by *PAGE4*, *SFRP4*, *APCDD1*, etc.) and subcluster 3 fibroblasts (marked by *GPX3*, *MYF5*, *CHODL*, etc.) were mostly recorded in the left Wilms tumor sample (Fig. 3B). Cell counts and detailed markers for each fibroblast subpopulation are listed in Table S2 and Fig. S2 (see online supplementary material). Compared to the Wilms tumor samples, fibroblasts in the normal sample from the right kidney were comparatively fewer in number. However, almost all these

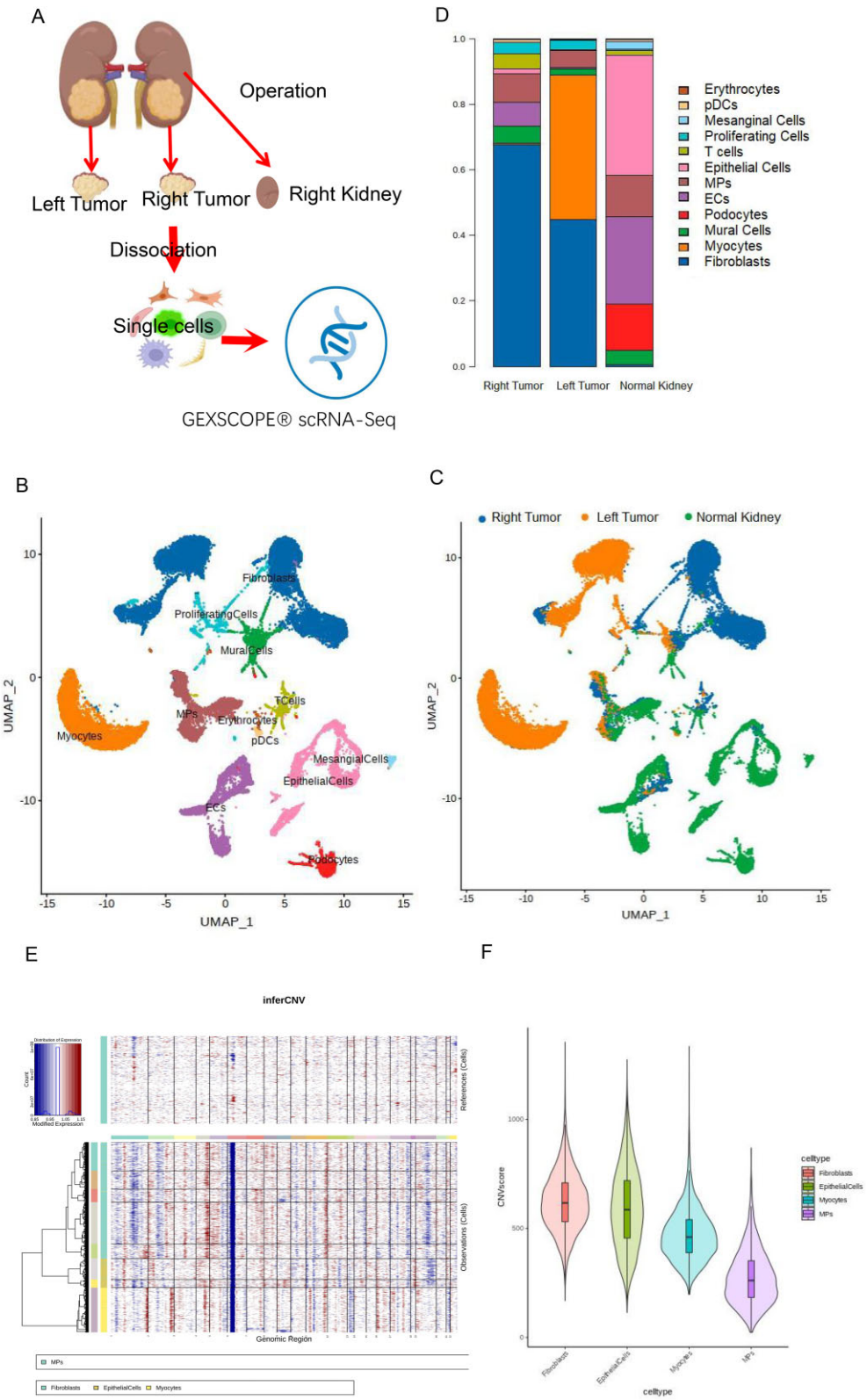

Figure 2: Single-cell RNA sequencing map from tumor and kidney tissues. **A**. Illustration of the scRNA-seq workflow in infant tumor and kidney tissue samples. **B**. Unbiased clustering of 31 135 cells reveals 12 cellular clusters. Clusters are distinguished by different colors. **C**. Distribution of cellular clusters in tumor and kidney tissue samples. **D**. Cell proportions in tumor and kidney tissue samples. Myocytes were increased in the left tumor tissue sample. **E–F**. CNV score in the major clusters (fibroblasts, epithelial cells, myocytes and MPs).

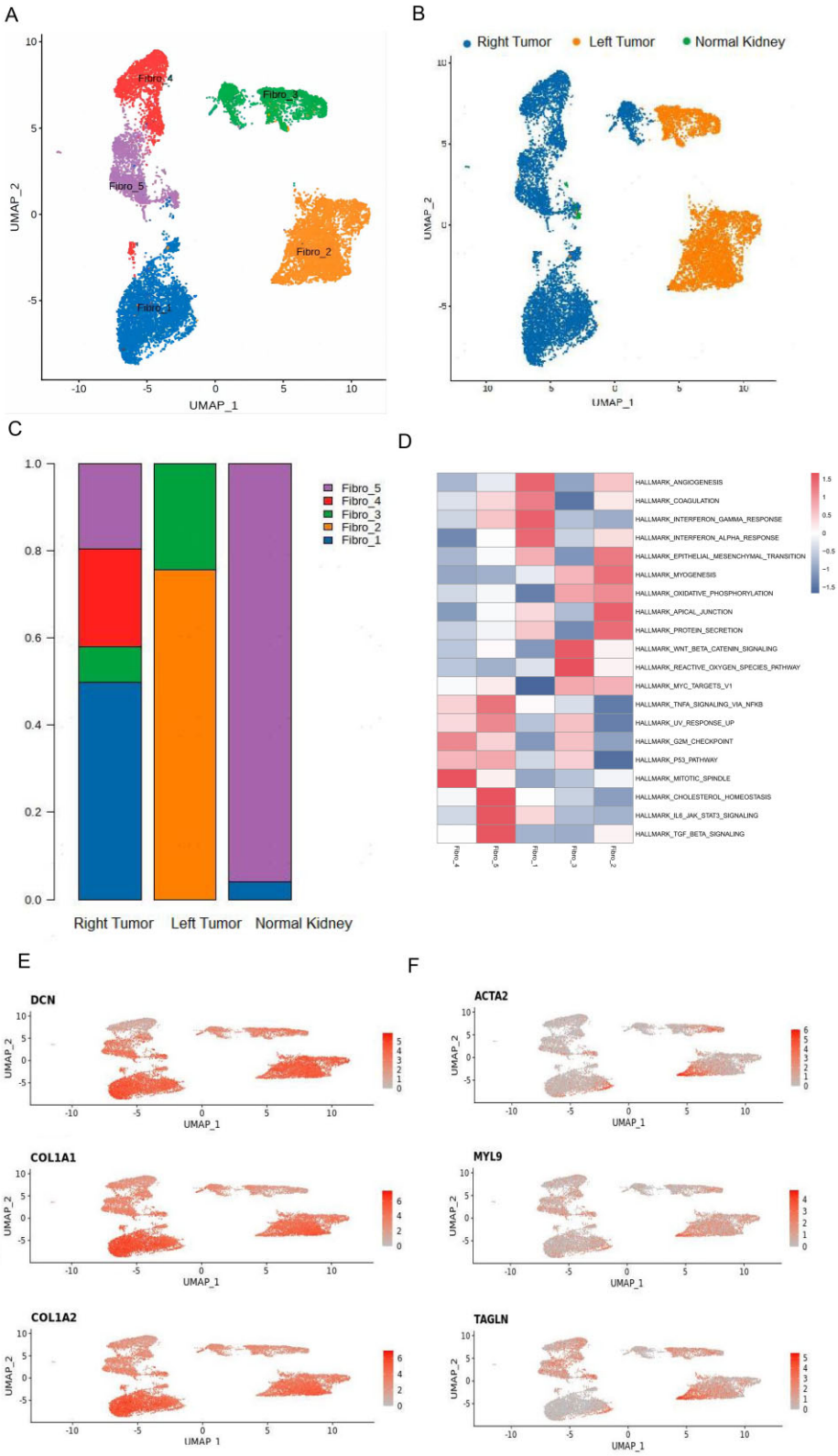

Figure 3: Tumor and kidney fibroblasts subcluster into distinct cell populations. **A**. Subclustering of tumor and kidney fibroblasts further identified five distinct subtypes. Color-coded UMAP plots are shown, and each fibroblast subcluster is defined. **B**. Distribution of fibroblast subclusters in tumor and kidney tissue samples. Fibroblasts were common in tumor tissues but few in normal kidney tissues. **C**. Fibroblast proportions in tumor and kidney tissue samples. Types 1, 4, and 5 were enriched in right tumor tissue samples. Meanwhile, types 2 and 3 were found in the left tumor tissues. Most fibroblasts in normal kidney tissues were type 5. **D**. Signaling pathways for fibroblasts. **E**. Gene signatures of fibroblasts in each subcluster. **F**. Gene signatures of myofibroblasts in each subcluster.

few fibroblasts were from subcluster 5, which was also observed in the right Wilms tumor (Fig. 3C). These fibroblast subclusters may harbor diverse functions (Fig. 3D). Subcluster 1/4/5 fibroblasts dominated in the right Wilms tumor sample. Subcluster 1 fibroblasts expressed mRNA profiles in angiogenesis, coagulation, IFN-γ response and IFN-α response. Subcluster 4 fibroblasts were characterized in pathways of TNF-α signal via NF-κB, UV response, G2M checkpoint, P53, and mitotic. Subcluster 5 fibroblasts were associated with cholesterol homeostasis, the IL-6-JAK-STAT3 pathway, and the TGF-β pathway. Most subcluster 2 and 3 fibroblast cells were in the left Wilms tumor sample, in which fibroblasts were closely associated with epithelial mesenchymal transition, apical junction, β-catenin, and reactive oxygen species pathway. Once activated, fibroblasts differentiate into myofibroblasts. As shown in Fig. 3E, the classical markers for fibroblasts, DCN, COL1A1, and COL1A2, were highly expressed in subclusters 1 and 2. However, only a few fibroblasts in subcluster 2 may be activated and express gene signatures, i.e. ACTA2, MYL9, and TAGLN (Fig. 3F). In sum, highly heterogeneous fibroblasts constituted the major cancerous population in Wilms tumor tissues.

Myocytes populated in left Wilms tumor tissue samples

Myocytes are muscle cells. As shown in Fig. 2D, myocytes were only recorded in Wilms tumor tissues, especially in the left Wilms tumor. The tumor myocytes could be further subclustered into four distinct subtypes (Fig. 4A). Subcluster 1 and 2 myocytes were common; in contrast, subcluster 3 and 4 myocytes were relatively fewer. Cell counts and detailed markers for each myocyte subpopulation are listed in Table S3 and Fig. S3 (see online supplementary material). Of note, most myocytes were from the left Wilms tumor (Fig. 4B). In the right Wilms tumor, subclusters 2 and 4 of myocytes were major. In the left Wilms tumor, however, subclusters 1 and 2 were overwhelmed (Fig. 4C). Using CytoTRACE [18], we predicted a higher developmental potential for myocytes in subclusters 2 and 4 than for myocytes in subclusters 1 and 3 (Fig. 4D). The right Wilms tumor was sensitive to the VAD regimen. In contrast, the left Wilms tumor was resistant to chemotherapy, which may lead to the accumulation of myocytes in the left Wilms tumor. To uncover the drug resistance associated with gene expression, we compared myocytes in different subclusters. CD44, a molecule associated with VAD drug resistance [19], was significantly higher in myocyte subclusters 2 and 3 from the left Wilms tumor (Fig. 4E). In contrast, TUBA1A, a molecule that reversely regulates VAD drug resistance [20], was significantly higher in myocyte subcluster 4 from the left Wilms tumor (Fig. 4F). Collectively, myocytes were popular in Wilms tumors, which may contribute to chemotherapy resistance.

Epithelial cells and endothelial cells prevailed in normal kidney tissues

Epithelial cells and endothelial cells play pivotal roles in kidney biological functions [21]. As shown in Fig. 2C–D, these cells were only recorded in the normal kidney tissue samples. The kidney epithelial cells could be further identified into six distinct subtypes [22, 23]: proximal tubule cells (PT), kidney loop of Henle epithelial cells (LOH), distal convoluted tubule cells (DCT), collecting duct principal cells (principal cells), collecting duct intercalated cells (intercalated cells), and IRX3$^+$ epithelial cells (Fig. 5A). Cell counts and detailed markers for each epithelial cell subpopulation are listed in Table S4 and Fig. S4 (see online supplementary material). Not surprisingly, most of the above-referenced epithelial cells were in normal kidney tissue samples (Fig. 5B). Few PT and IRX3$^+$ epithelial cells were recorded in the right Wilms tumor samples. Meanwhile, DCT and PT were the most common epithelial cells in normal kidney tissue samples (Fig. 5C). As analysed in the CNV score (Fig. 2E–F), epithelial cells may be cancerous, which raised the possibility that cancerous cells in the Wilms tumor may have originated from epithelial cells. In the renal tumor scRNA-Seq, PT cells may transform into clear cell renal cell carcinoma [11]. To explore the potential differentiation of PT cells, we performed trajectory analysis. As shown in Fig. 5D–E, PT cells branched to either LOH, DCT, principal cells, intercalated cells, or IRX3$^+$ epithelial cells. We could not exclude the possibility that Wilms tumors in DDS may originate from kidney epithelial cells. Similarly, kidney endothelial cells could be further identified into 5 distinct subtypes: glomerular endothelial cells (glomerular ECs), venous endothelial cells (VECs), arterial endothelial cells (AECs), capillary endothelial cells (Cap ECs) and lymphatic endothelial cells (LECs) (Fig. 5F). Cell counts and detailed markers for each epithelial cell subpopulation are listed in Table S5 and Fig. S5 (see online supplementary material). Few endothelial cells were observed in the right and left Wilms tumors (Fig. 5G). Moreover, the distribution of endothelial cell subtypes varied. In right and left Wilms tumors, VECs and Cap ECs were most common; in contrast, Glomerular ECs and Cap ECs prevailed in normal kidney tissues (Fig. 5H). Taken together, epithelial cells and endothelial cells were the indispensable cellular components in normal kidney tissues, and cancer cells in Wilms tumors may be from these normal cells, i.e. epithelial cells .

Mononuclear phagocyte (MP) heterogenicity in the Wilms tumor microenvironment

The tumor microenvironment supports tumor initiation and progression. Immune cells are key modulators in the tumor microenvironment. As shown in Fig. 3, pDCs, T cells and MPs were the most common immune cells in kidney tissues. Among these immune cells, MPs are the only immune cells found not only in normal kidney tissues but also in Wilms tumors. To delve into the roles of MPs in tumorigenesis, we subclustered MPs into five distinct subtypes: macrophages, monocytes, conventional type 1 dendritic cells (cDC1), conventional type 2 dendritic cells (cDC2), and mature dendritic cells (Fig. 6A). Cell counts and detailed markers for each MP subpopulation are listed in Table S6 and Fig. S6 (see online supplementary material). In comparison, monocytes and cDC2s were enriched in the normal kidney tissue; macrophages were more popular in the Wilms tumor tissues (Fig. 6B–C). Cell counts and detailed markers for each macrophage subcluster are listed in Table S7 and Fig. S7 (see online supplementary material). To further understand the differentiation processes, we performed trajectory analysis. As shown in Fig. 6D–E, monocytes differentiated into macrophages; especially, monocytes differentiated into macrophages subclusters 1 and 2 in the right tumors; and macrophages subclusters 3 and 4 from monocytes were in the left tumors. In the differentiation from monocytes to macrophages, the levels of *FCN1*, *LYZ*, *TIMP1*, *PLAUR*, and *VCAN* decreased; meanwhile, the levels of *LGMN*, *PLD3*, and *RGS1* increased (Fig. 6F). Together, we revealed the heterogenicity of MPs in the kidney and Wilms tumor tissues, which may interact with tumor cells and promote tumor progression.

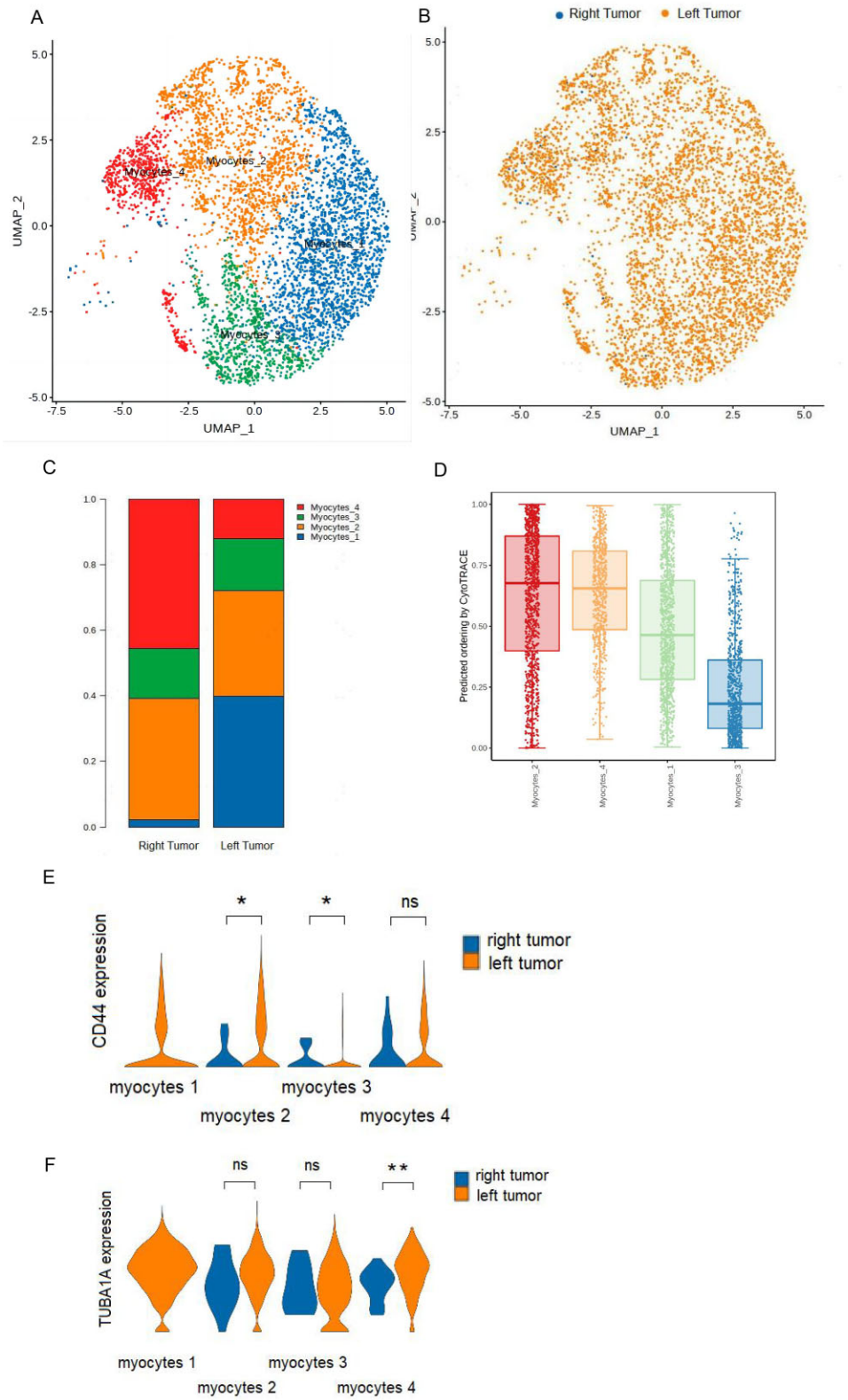

Figure 4: Tumor myocytes subcluster into distinct cell populations. **A**. Sub-clustering of tumor myocytes further identified four distinct subtypes. Color-coded UMAP plots are shown, and each myocyte subcluster is defined. **B**. Distribution of myocyte subclusters in tumor tissue samples. Myocytes were mostly recorded in left tumor tissues. **C**. Myocyte proportions in right and left tumor tissue samples. Type 1 myocytes were enriched in left tumor tissue samples. **D**. Predicted ordering in different subtypes of myocytes. **E–F**. Drug-resistance analysis of associated genes, *CD44* and *TUBA1A*, in myocytes against incristine, doxorubicin, and dexamethasone. *$P < 0.05$.

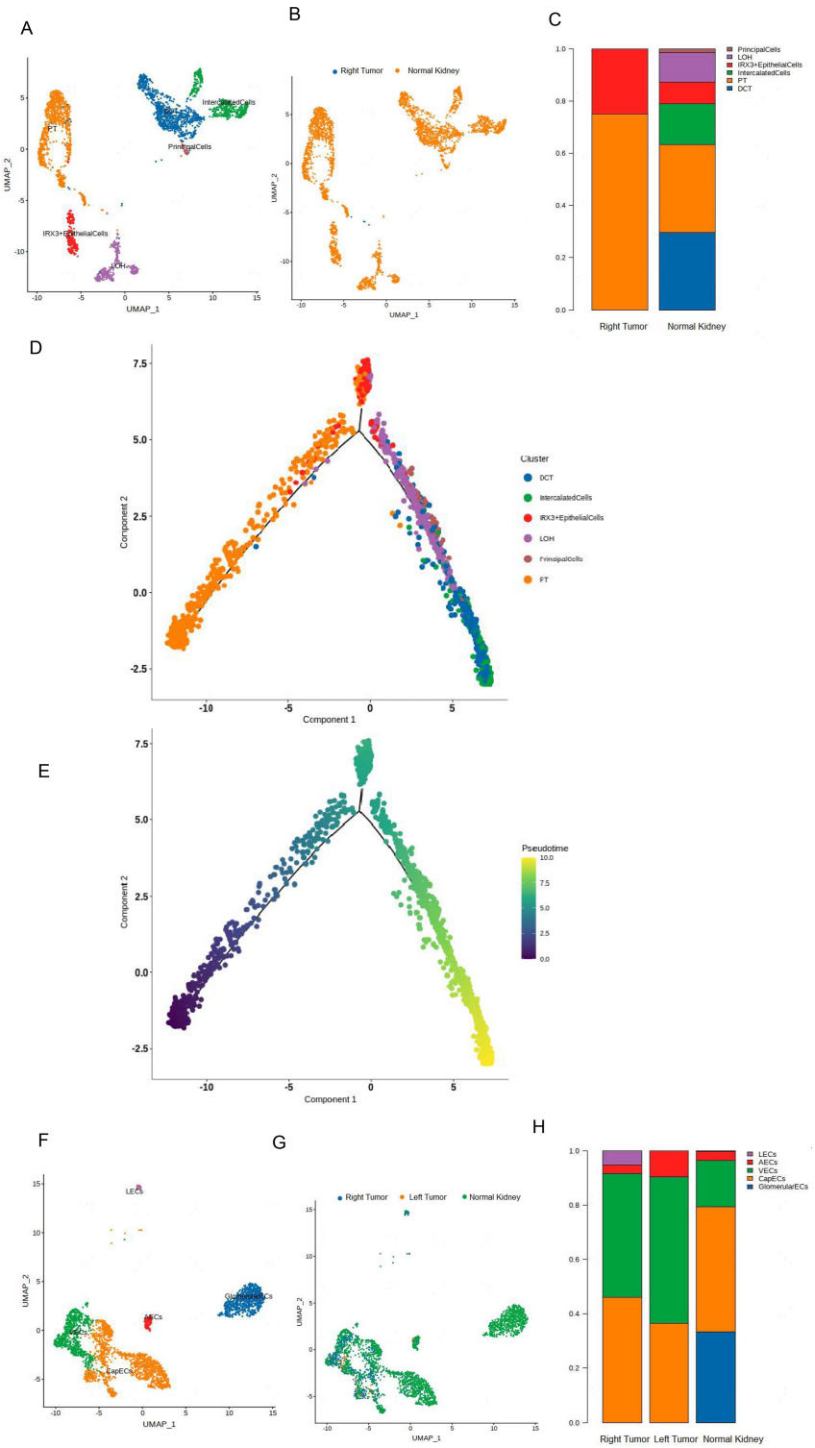

Figure 5: Epithelial cells and endothelial cells dominate in normal kidney tissue samples. **A**. Subclustering of tumor and kidney epithelial cells further identified six distinct subtypes: proximal tubule cells (PT), kidney loop of Henle epithelial cells (LOH), distal convoluted tubule cells (DCT), collecting duct principal cells (PrincipalCells), collecting duct intercalated cells (intercalated cells), and IRX3 + epithelial cells. Color-coded UMAP plots are shown, and each epithelial cell subcluster is defined. **B**. Distribution of epithelial cell subclusters in tumor and kidney tissue samples. Epithelial cells were common in normal kidney tissues but few in tumor tissues. **C**. Epithelial cell proportions in tumor and kidney tissue samples. All six epithelial cell subtypes were recorded in normal kidney tissue samples. Proximal tubule cells predominate in the right tumor tissue sample. **D–E**. Trajectory analysis of epithelial cells. **F**. Sub-clustering of tumor and kidney endothelial cells further identified five distinct subtypes: glomerular endothelial cells (glomerularECs), venous endothelial cells (VECs), arterial endothelial cells (AECs), capillary endothelial cells (CapECs), and lymphatic endothelial cells (LECs). Color-coded UMAP plots are shown, and each endothelial cell subcluster is defined. **G**. Distribution of endothelial cell subclusters in tumor and kidney tissue samples. Endothelial cells were common in normal kidney tissues but few in tumor tissues. **H**. Endothelial cell proportions in tumor and kidney tissue samples. Lymphatic endothelial cells were observed in right tumor tissue samples but not in normal kidney tissues.

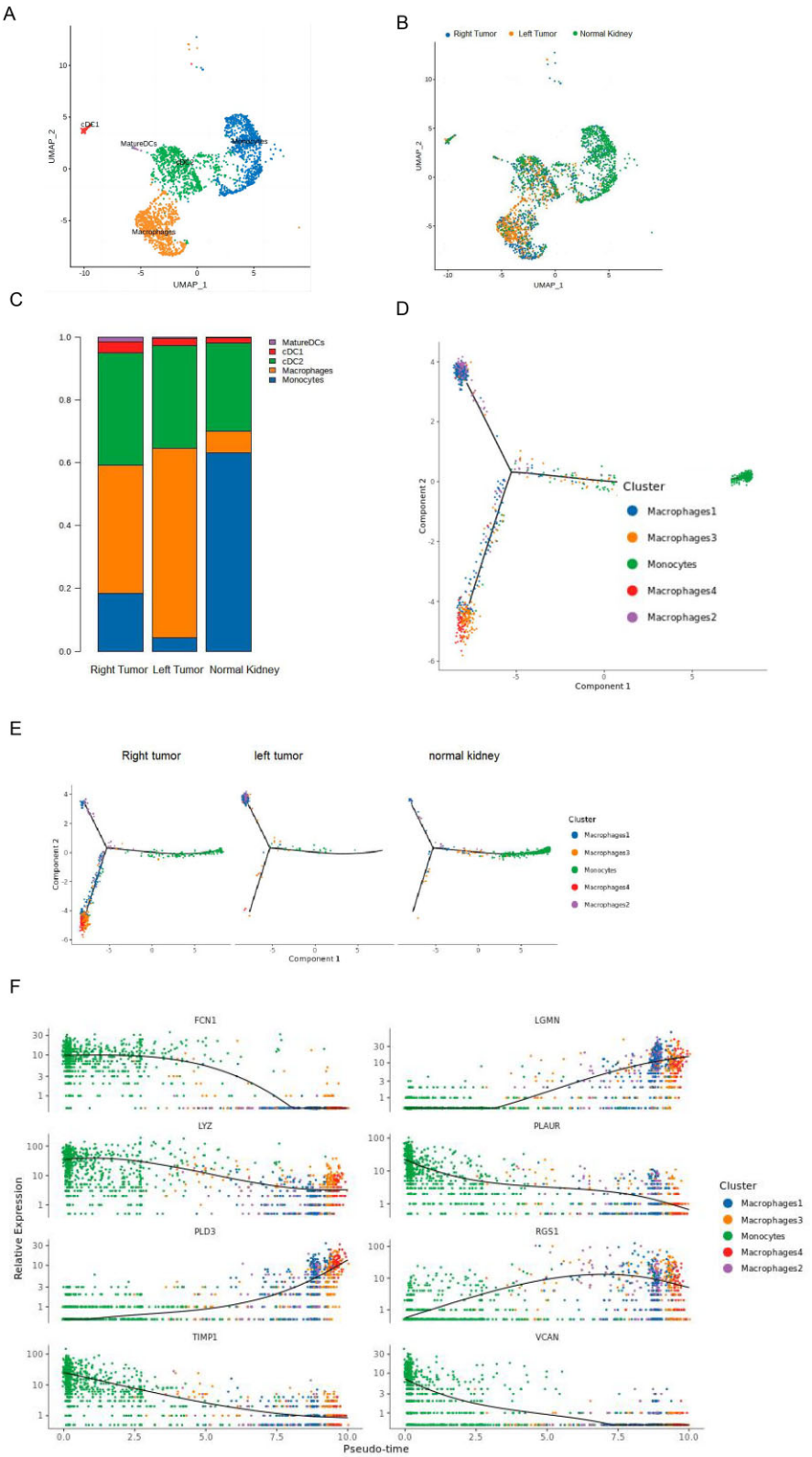

Figure 6: Tumor and kidney mononuclear phagocytes (MPs) subcluster into distinct cell populations. **A**. Subclustering of tumor and kidney MPs further identified five distinct subtypes: macrophages, monocytes, conventional type 1 dendritic cells (cDC1), conventional type 2 dendritic cells (cDC2), and mature dendritic cells. Color-coded UMAP plots are shown, and each endothelial cell subcluster is defined. **B**. Distribution of MP subclusters in tumor and kidney tissue samples. Monoytes are almost absent in the left tumor tissue samples. **C**. MP cell proportions in tumor and kidney tissue samples. Compared with normal kidney tissue samples, tumor tissue samples have increased macrophages. **D–E**. Trajectory-based differential expression analysis for monocytes and macrophage subclusters in tumor and kidney tissue samples. **F**. Transcriptional changes in monocytes and macrophages in the trajectory analysis.

Macrophages communicated with tumor cells

Macrophages play essential roles in the tumor microenvironment. As described above, CNVs in fibroblasts, epithelial cells, and myocytes were much higher than those in macrophages. Using CellphoneDB [24], we predicted the cell–cell communication between macrophages and other cells, especially fibroblasts, epithelial cells, and myocytes. In general, the crosstalk between macrophages and fibroblasts from either Wilms tumors (left, right) or normal kidney tissues seemed similar (Fig. 7A). In the listed 20 interactions, 19 receptor-ligand bindings were similar in the right tumor, normal kidney tissue, and left tumor. However, TNFRSF1A-GRN was recorded in macrophage-fibroblasts in the left Wilms tumor and normal kidney but almost vanished in the right Wilms tumor sample. Interactions between macrophages and epithelial cells were comparable in the right tumor, normal kidney tissue, and left tumor samples. One key change was that TNFSF10-RIPK1 may be increased in the right tumor tissues (Fig. 7B). Myocytes were almost only recorded in the Wilms tumor tissues. The bilateral Wilms tumor samples were similar in the interactions between macrophages and myocytes (Fig. 7C). Above all, macrophages communicate with fibroblasts, epithelial cells, and myocytes, which may contribute to tumor progression.

DISCUSSION

In the present study, a 6-month-old boy (46, XY) with bilateral Wilms tumors and false hermaphroditism (hypospadias, labia minora and vaginal opening) was diagnosed with DDS. WT1 mutation is the culprit for Wilms tumor and associated syndromes, i.e. DDS, WAGR syndrome (Wilms tumor, aniridia, genitourinary anomalies, and impaired intellectual development) and Beckwith–Wiedemann syndrome. The WT1 gene includes 10 exons: exons 1 to 6 encoding the N-terminal domain for transactivation and exons 7 to 10 encoding the C-terminal domain for DNA binding. Here, we found a novel frameshift nonsense mutation in exon 1 of WT1: p.F185fs*118 (p.Phe185fsTer118). The premature termination of exon 1 may disable the inhibitory functions of WT1, which may accelerate kidney tumor progression in this 6-month boy. The roles and mechanisms of p.F185fs*118 warrant further investigation in cell and animal models [25] of Wilms tumor and DDS.

To explore the cellular components of Wilms tumors and kidney tissue in DDS, we performed single-cell RNA-Seq. In consideration of cell numbers and potential functions, we focused on the top 3 nonimmune cells (fibroblasts, myocytes, and epithelial cells) and the top 1 immune cell, i.e. MPs. Epithelial cells were the most common type in the normal kidney tissue sample. In contrast, Wilms tumor tissue samples were confluent with fibroblasts and myocytes but lacked epithelial cells. CNVs of certain genes are involved with cancer progression [26]. Compared with MPs, all these nonimmune cells had higher CNVs, indicating that they may be cancerous. Our observation supported the hypothesis that cancer cells in Wilms tumor may originate from aberrant fetal cells [11], i.e. epithelial cells. In fact, WT1 in Wilms tumor induced the transformation of epithelial cells into fibroblasts [27]. Myocytes may also originate from epithelial cells. For example, epicardial cells, epithelial cells in the heart, have the potential to differentiate into cardiac myocytes [28]. We could not exclude the possibility that epithelial cells were cancerous and transdifferentiate into fibroblasts and myocytes in the Wilms tumor. As similar as these non-immune cells, MPs also play essential roles in the tumor micro-environment. Monocytes differentiated into

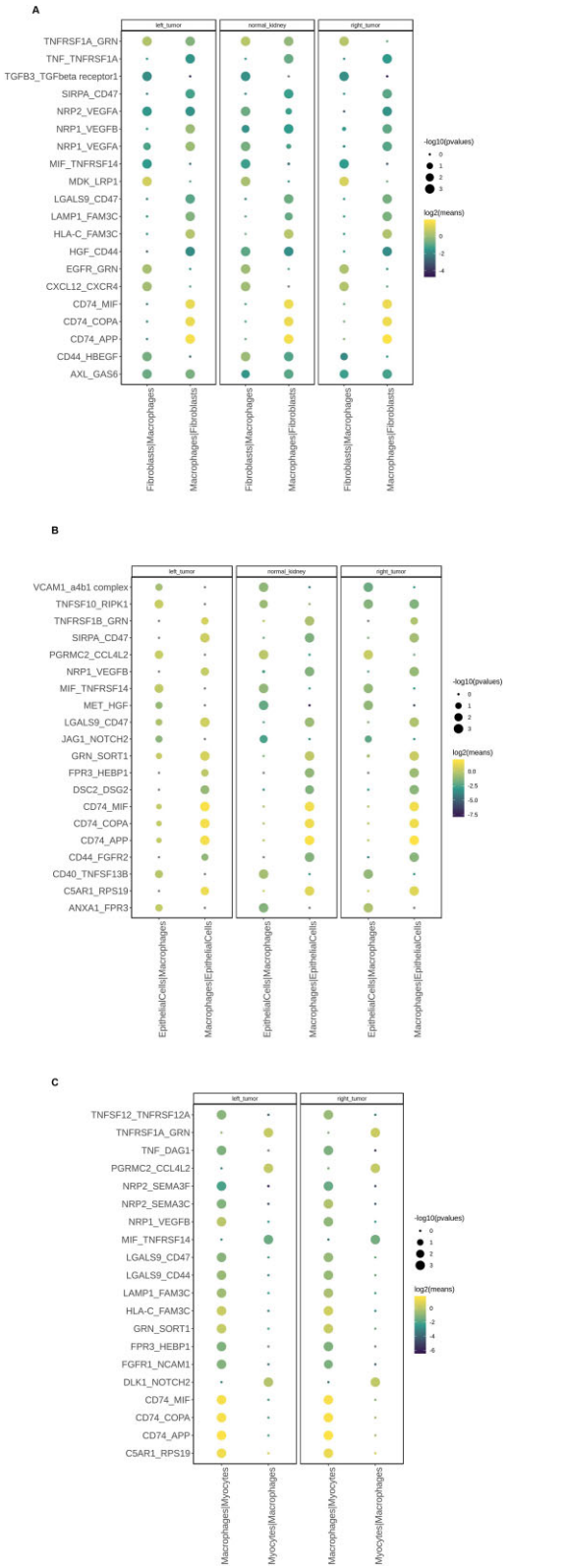

Figure 7: Cell-to-cell communications between macrophages and fibroblasts, epithelial cells, and myocytes in Wilms tumors and normal kidney tissues. **A**. Overview of selected ligand–receptor interactions between macrophages and fibroblasts. **B**. Overview of selected ligand–receptor interactions between macrophages and epithelial cells. **C**. Overview of selected ligand–receptor interactions between macrophages and myocytes. *P* values are indicated by circle size (permutation test). The means of the average expression level of interactions are indicated by color.

macrophages, accompanied with decreased levels of *FCN1*, *LYZ*, *TIMP1*, *PLAUR*, and *VCAN*, and increased levels of *LGMN*, *PLD3*, and *RGS1*. These genes are involved with macrophage differentiation and tumor progression. For example, $FCN1^{+}$ macrophages exhibited proinflammatory phenotypes [29]; FCN1 reduction in macrophages may promote cancer progression.

As the guiding management principles [30, 31], the boy was treated with neoadjuvant chemotherapy and nephron-sparing surgery. Wilms tumor on the right was sensitive to VAD regimen chemotherapy. In contrast, the left Wilms tumor was resistant. The striking difference in cellular components in the bilateral Wilms tumors was that myocytes populated the left Wilms tumors. Single-cell transcriptional changes may help uncover the mechanisms of drug resistance [32]. To explore the molecules involved in VAD drug resistance, we compared multiple genes and found that *CD44* [19] and *TUBA1A* [20] were higher in the myocyte subclusters from left Wilms tumor, suggesting a complicated evolution of cancer cells upon chemotherapy. In the cells cross-talking analysis, Galectin 9 encoded by *LAGLS9* in macrophages interacted with CD44 in myocytes. Galectin 9 regulates tumor immune microenvironment and cancer progression [33]. Targeting CD44 and TUBA1A may improve the efficiency of VAD chemotherapy against Wilms tumors.

This study had some limitations. First, the research lacked some important controls, i.e. Wilms tumors from other infants with similar ages and normal kidney tissues from other infants. However, renal tumors in 6-month-old infants are less likely to be Wilms tumors [34], which increases the difficulty of including appropriate Wilms tumor controls in DDS research. Second, the sample size was small. Future studies with more DDS patients are definitely needed. DDS is a rare disease, even fewer than Wilms tumors. Frozen samples from DDS patients may be explored by single-nucleus RNA sequencing, which is more suitable for frozen samples than single-cell RNA sequencing [35]. Third, the cellular phenotype and potential functions revealed by single-cell RNA sequencing should be verified using other methods. Due to the paucity of clinical samples, we did not have enough tissue for multicolor flow cytometry to verify the speculations. Perhaps DDS animal models should be established.

In conclusion, we provided the first single-cell transcriptome of bilateral Wilms tumors and normal kidney tissues in a 6-month-old boy with a rare disease, DDS. Fibroblasts and myocytes in Wilms tumors may be from kidney epithelial cells, which were almost absent in the tumor samples. Upon chemotherapy, myocytes developed drug resistance, which was characterized by altered levels of *CD44* and *TUBA1A*. The communications between macrophages and cancerous fibroblasts, epithelial cells and myocytes may contribute to tumor progression.

SUPPLEMENTARY DATA

Supplementary data are available at *ckj* online.

ACKNOWLEDGEMENTS

We thank Chigene Translational Medical Research Center (Beijing, China) for their assistance in whole exome sequencing and analysis. We thank Singleron Biotechnologies (Nanjing, China) for their cooperation in single-cell RNA sequencing and bioinformatics analysis. This study was approved by the Medical Ethics Committee of Children's Hospital Affiliated to Nanjing Medical University (202301001-1). Written informed consent was signed by the parents.

FUNDING

This work was supported by the National Natural Science Foundation of China (82171705, 82171738).

AUTHORS' CONTRIBUTIONS

(I) Conception and design: T.L., M.Z. (II) Administrative support: T.L., R.C. (III) Screening and sampling: J.Z., H.W., X.G., Q.S. (IV) Collection and assembly of data: T.L., J.Z. (V) Data analysis and visualization: M.Z., R.C. (VI) Manuscript writing—original draft: T.L., M.Z. (VII) Manuscript writing—review and editing: R.C., M.Z. All authors listed have made substantial, direct, and intellectual contributions to the work and approved it for publication.

DATA AVAILABILITY STATEMENT

The data presented are publicly accessible in the Gene Expression Omnibus database (GSE223373). The data that support the findings of this study are available from the corresponding authors upon reasonable request.

CONFLICT OF INTEREST STATEMENT

The authors declare no conflict of interest.

REFERENCES

1. Mueller RF. The Denys-Drash syndrome. *J Med Genet* 1994;**31**:471–7. https://doi.org/10.1136/jmg.31.6.471
2. Al-Hussain T, Ali A, Akhtar M. Wilms tumor: an update. *Adv Anat Pathol* 2014;**21**:166–73. https://doi.org/10.1097/PAP.0000000000000017
3. Little M, Wells C. A clinical overview of WT1 gene mutations. *Hum Mutat* 1997;**9**:209–25. https://doi.org/10.1002/(SICI)1098-1004(1997)9:3%3c209::AID-HUMU2%3e3.0.CO;2-2
4. Guaragna MS, Ledesma FL, Manzano VZ *et al*. Bilateral Wilms tumor in a child with Denys-Drash syndrome: novel frameshift variant disrupts the WT1 nuclear location signaling region. *J Pediatr Endocrinol Metab* 2022;**35**:837–43. https://doi.org/10.1515/jpem-2021-0673
5. Heathcott RW, Morison IM, Gubler MC *et al*. A review of the phenotypic variation due to the Denys-Drash syndrome-associated germline WT1 mutation R362X. *Hum Mutat* 2002;**19**:462. https://doi.org/10.1002/humu.9031
6. Termuhlen AM, Tersak JM, Liu Q *et al*. Twenty-five year follow-up of childhood Wilms tumor: a report from the Childhood Cancer Survivor Study. *Pediatr Blood Cancer* 2011;**57**:1210–6. https://doi.org/10.1002/pbc.23090
7. Roca N, Muñoz M, Cruz A *et al*. Long-term outcome in a case series of Denys-Drash syndrome. *Clin Kidney J* 2019;**12**:836–9. https://doi.org/10.1093/ckj/sfz022
8. Kreidberg JA, Sariola H, Loring JM *et al*. WT-1 is required for early kidney development. *Cell* 1993;**74**:679–91. https://doi.org/10.1016/0092-8674(93)90515-R
9. Schumacher VA, Jeruschke S, Eitner F *et al*. Impaired glomerular maturation and lack of VEGF165b in Denys-Drash syndrome. *J Am Soc Nephrol* 2007;**18**:719–29. https://doi.org/10.1681/ASN.2006020124
10. Wagner K-D, El Maï M, Ladomery M *et al*. Altered VEGF splicing isoform balance in tumor endothelium involves activation of splicing factors Srpk1 and Srsf1 by the Wilms tumor suppressor Wt1. *Cells* 2019;**8**:41. https://doi.org/10.3390/cells8010041

11. Young MD, Mitchell TJ, Vieira Braga FA *et al*. Single-cell transcriptomes from human kidneys reveal the cellular identity of renal tumors. *Science* 2018;**361**:594–9. https://doi.org/10.1126/science.aat1699
12. Young MD, Mitchell TJ, Custers L *et al*. Single cell derived mRNA signals across human kidney tumors. *Nat Commun* 2021;**12**:3896. https://doi.org/10.1038/s41467-021-23949-5
13. Xu J, Shen C, Lin W *et al*. Single-cell profiling reveals transcriptional signatures and cell-cell crosstalk in anti-PLA2R positive idiopathic membranous nephropathy patients. *Front Immunol* 2021;**12**:683330. https://doi.org/10.3389/fimmu.2021.683330
14. Liao Y, Smyth GK, Shi W. featureCounts: an efficient general purpose program for assigning sequence reads to genomic features. *Bioinformatics* 2014;**30**:923–30. https://doi.org/10.1093/bioinformatics/btt656
15. Satija R, Farrell JA, Gennert D *et al*. Spatial reconstruction of single-cell gene expression data. *Nat Biotechnol* 2015;**33**:495–502. https://doi.org/10.1038/nbt.3192
16. Butler A, Hoffman P, Smibert P *et al*. Integrating single-cell transcriptomic data across different conditions, technologies, and species. *Nat Biotechnol* 2018;**36**:411–20. https://doi.org/10.1038/nbt.4096
17. Subramanian A, Tamayo P, Mootha VK *et al*. Gene set enrichment analysis: a knowledge-based approach for interpreting genome-wide expression profiles. *Proc Natl Acad Sci U S A* 2005;**102**:15545–50. https://doi.org/10.1073/pnas.0506580102
18. Gulati GS, Sikandar SS, Wesche DJ *et al*. Single-cell transcriptional diversity is a hallmark of developmental potential. *Science* 2020;**367**:405–11. https://doi.org/10.1126/science.aax0249
19. Phuc PV, Chinh Nhan PL, Nhung TH *et al*. Downregulation of CD44 reduces doxorubicin resistance of CD44CD24 breast cancer cells. *Onco Targets Ther* 2011;**4**:71–78. https://doi.org/10.2147/OTT.S21431
20. Horbach L, Sinigaglia M, Da Silva CA *et al*. Gene expression changes associated with chemotherapy resistance in Ewing sarcoma cells. *Mol Clin Oncol* 2018;**8**:719–24. https://doi.org/10.3892/mco.2018.1608
21. Balzer MS, Rohacs T, Susztak K. How many cell types are in the kidney and what do they do? *Annu Rev Physiol* 2022;**84**:507–31. https://doi.org/10.1146/annurev-physiol-052521-121841
22. Qiu C, Huang S, Park J *et al*. Renal compartment-specific genetic variation analyses identify new pathways in chronic kidney disease. *Nat Med* 2018;**24**:1721–31. https://doi.org/10.1038/s41591-018-0194-4
23. Xu Y, Kuppe C, Perales-Patón J *et al*. Adult human kidney organoids originate from CD24(+) cells and represent an advanced model for adult polycystic kidney disease. *Nat Genet* 2022;**54**:1690–701. https://doi.org/10.1038/s41588-022-01202-z
24. Xu K, Wang R, Xie H *et al*. Single-cell RNA sequencing reveals cell heterogeneity and transcriptome profile of breast cancer lymph node metastasis. *Oncogenesis* 2021;**10**:66. https://doi.org/10.1038/s41389-021-00355-6
25. Ratelade J, Arrondel C, Hamard G *et al*. A murine model of Denys-Drash syndrome reveals novel transcriptional targets of WT1 in podocytes. *Hum Mol Genet* 2010;**19**:1–15. https://doi.org/10.1093/hmg/ddp462
26. Shao X, Lv N, Liao J *et al*. Copy number variation is highly correlated with differential gene expression: a pan-cancer study. *BMC Med Genet* 2019;**20**:175. https://doi.org/10.1186/s12881-019-0909-5
27. Sampson VB, David JM, Puig I *et al*. Wilms tumor protein induces an epithelial-mesenchymal hybrid differentiation state in clear cell renal cell carcinoma. *PLoS One* 2014;**9**:e102041. https://doi.org/10.1371/journal.pone.0102041
28. Wu SM, Fujiwara Y, Cibulsky SM *et al*. Developmental origin of a bipotential myocardial and smooth muscle cell precursor in the mammalian heart. *Cell* 2006;**127**:1137–50. https://doi.org/10.1016/j.cell.2006.10.028
29. Chen XX, Gao Y, Xie J *et al*. Identification of FCN1 as a novel macrophage infiltration-associated biomarker for diagnosis of pediatric inflammatory bowel diseases. *J Transl Med* 2023;**21**. https://doi.org/10.1186/s12967-023-04038-1
30. Charlton J, Irtan S, Bergeron C *et al*. Bilateral Wilms tumour: a review of clinical and molecular features. *Expert Rev Mol Med* 2017;**19**:e8. https://doi.org/10.1017/erm.2017.8
31. Murphy AJ, Davidoff AM. Bilateral Wilms tumor: a surgical perspective. *Children (Basel)* 2018;**5**. https://doi.org/10.3390/children5100134
32. Aissa AF, Islam ABMMK, Ariss MM *et al*. Single-cell transcriptional changes associated with drug tolerance and response to combination therapies in cancer. *Nat Commun* 2021;**12**:1628. https://doi.org/10.1038/s41467-021-21884-z
33. Mariño KV, Cagnoni AJ, Croci DO *et al*. Targeting galectin-driven regulatory circuits in cancer and fibrosis. *Nat Rev Drug Discov* 2023;**22**:295–316. https://doi.org/10.1038/s41573-023-00636-2
34. Glick RD, Hicks MJ, Nuchtern JG *et al*. Renal tumors in infants less than 6 months of age. *J Pediatr Surg* 2004;**39**:522–5. https://doi.org/10.1016/j.jpedsurg.2003.12.007
35. Fischer J, Ayers T. Single nucleus RNA-sequencing: how it's done, applications and limitations. *Emerg Top Life Sci* 2021;**5**:687–90. https://doi.org/10.1042/ETLS20210074

Received: 19.3.2023; Editorial decision: 24.10.2023